D-^{3}He BURNING, SECOND STABILITY REGION, AND THE IGNITOR EXPERIMENT

EXPERIMENTAL DEVICES

KEYWORDS: *second stability region, ignition experiment, D-^{3}He burning*

B. COPPI, P. DETRAGIACHE,* S. MIGLIUOLO, M. NASSI,*
and B. ROGERS *Massachusetts Institute of Technology*
Cambridge, Massachusetts 02139

Received July 7, 1993
Accepted for Publication December 2, 1993

The Ignitor experiment has been designed to achieve fusion burn and ignition conditions in a high-density deuterium-tritium (D-T) plasma with a compact high magnetic field confinement configuration. The recent addition of a powerful system of radio-frequency heating to the design of Ignitor allows the investigation of physics issues relevant to advanced D-^{3}He reactors and the second stability region for finite-β plasmas. To maximize the production of D-^{3}He power, a lower density regime is considered (e.g., $n_0 = 3 \times 10^{20}$ m^{-3}) than that found to be optimal for D-T ignition ($n_0 = 1 \times 10^{21}$ m^{-3}). This allows a relatively large population of ^{3}He nuclei at high energies $\geq$0.65 MeV to be produced by a high density of injected power at the ^{3}He ion cyclotron frequency (up to 18 MW injected in the plasma column of volume $\leq$10 m^3).

The investigation of second stability region access can be carried out in relatively low magnetic field and plasma current regimes with the added benefit that the duration of the plasma discharge can be extended over relatively long times. In fact, the Ignitor magnets can be brought down to an initial temperature of 30 K by gas-helium cooling. The low aspect ratio ($\simeq$2.8) and elongated plasma cross section of Ignitor make it suitable to reach both finite-β conditions and interesting plasma regimes at the same time.

The Candor concept is the next step in the evolution of the Ignitor program. Candor is capable of producing plasma currents up to 25 MA with toroidal magnetic fields $B_T \simeq 13$ T. Unlike Ignitor, Candor would operate with values of β_p around 1.5 and with the central part of the plasma column in the second stability region. The D-^{3}He ignition in this case can be reached by a combination of ICRF heating and alpha-particle heating due to D-T fusion reactions.

I. THE IGNITOR EXPERIMENT

I.A. Objectives

Since its original proposal in 1975 (Ref. 1), the Ignitor experiment has undergone a process of continuing development of its regimes of operation[1-16] and engineering design,[17-24] motivated by the results of experiments and improvements in our understanding of the physics of high-temperature plasmas.

Its main goals include the following:

1. study the containment of the produced alpha particles and the plasma heating generated by them
2. investigate collective modes and transport processes that characterize deuterium-tritium (D-T) fusion burning plasmas
3. attain fusion burning and ignition conditions at relatively low peak temperatures ($T_{i0} \simeq T_{e0} \leq$ 15 keV) with values of the confinement parameter $n_0\tau_E \geq 4 \times 10^{20}$ s/m^3, avoiding the need for reliance on an injected heating system. (Here

*Permanent address: ENEA, corso M. D'Azeglio 42, I-10125 Torino, Italy.

n_0 is the peak plasma density and τ_E is the energy replacement time)

4. study the effectiveness of a suitable ion cyclotron resonance frequency (ICRF) heating system, with $P_{rf} \leq 18$ MW, in accelerating the approach to burning conditions and in controlling the evolution (central peaking) of the toroidal current density profile to avoid the possible onset of sawtooth oscillations
5. test diagnostic systems for burning plasmas
6. identify new methods for control, heating, and fueling of high-density plasmas.

Furthermore, the expected plasma parameters, the flexible set of poloidal field coils and the availability of an ICRF system and pellet injector make Ignitor suitable for exploring the following:

1. subignited ($Q \leq 5$) (the quantity Q is defined in the caption of Table V) fusion burning, high field plasma regimes with a relatively wide range of temperatures and densities
2. the possibility of producing significant power from D-^{3}He fusion reactions, using ICRF heating to enhance reactivity in a deuterium plasma with a ^{3}He minority
3. the access to the high-β second stability region by operating at low field and plasma currents with substantial ICRF heating. In this case, the plasma column can be maintained over relatively long intervals in view of the fact that the Ignitor magnets are cooled down to 30 K. In this respect, Ignitor is as suitable as a superconducting facility to explore long pulse operation, while having a set of desirable geometrical characteristics such as its low aspect ratio.

I.B. Physics Basis

The Ignitor experiment was conceived on the basis of well-known properties of high-density plasmas, good confinement, and high purity, which had been discovered by the high field machines Alcator/Alcator-C at the Massachusetts Institute of Technology[25] and Frascati Torus/Frascati Torus Upgrade (FT/FTU) in Italy. Furthermore, these results have been confirmed in the Tokamak Fusion Test Reactor (TFTR) and other advanced experiments. Compact high field experiments were the first[1] to be proposed in order to achieve fusion ignition conditions on the basis of existing technology and the known properties of high-density plasmas. The reference plasma dimensions and parameters of Ignitor Ult are reported in Table I, and the machine's key elements are given in Fig. 1.

The Ignitor machine parameters have been chosen in order to obtain[4]

TABLE I

Reference Design Parameters of the Ignitor Ult Experiment

$R_0 = 1.32$ m	Major radius of the plasma column
$a \times b = 0.47 \times 0.87$ m^2	Minor radii of the plasma cross section
$R_0/a = 2.8$	Aspect ratio of the plasma column
$\delta_G = 0.4$	Triangularity of the plasma cross section
$I_p \leq 12$ MA	Plasma current in the toroidal direction
$I_\theta \leq 9$ MA	Plasma current in the poloidal direction
$B_T \leq 13$ T	Vacuum toroidal field at R_0
$\Delta B_T \leq 1.5$ T	Paramagnetic (additional) field produced by I_θ
$\langle J_\phi \rangle \leq 9.3$ MA/m^2	Average toroidal current density
$\bar{B}_p \leq 3.75$ T	Mean poloidal field
$I_p \bar{B}_p \leq 45$ MN/m	Confinement strength parameter
$q_\psi = 3.3$	Edge magnetic safety factor at $I_p = 12$ MA
$V_0 = 10$ m^3	Plasma volume
$S_0 = 36$ m^2	Plasma surface area
$P_{rf} \leq 18$ MW	Injected heating power (ICRF with $100 \leq \nu \leq 210$ MHz)

1. a high peak plasma density ($n_0 \simeq 10^{21}$ m^{-3}). The maximum plasma density that can be supported in an ohmically heated toroidal plasma has been observed to correlate roughly with the ratio B_T/R_0. On the basis of results of the Alcator C machine, where $n_0 \simeq 2 \times 10^{21}$ m^{-3} was achieved with $B_T \simeq 12.5$ T and $R_0 \simeq 0.64$ m, and those of the TFTR machine at Princeton, where even larger ratios of $n_0 R_0/B_T$ were achieved, a configuration with $R_0 \simeq 1.3$ m and $B_T \simeq 13$ T should be able to reliably sustain densities of 10^{21} m^{-3}. Furthermore, if the density correlates with the volume-averaged toroidal current density $\langle J_\phi \rangle$, experimental results suggest that the value of $\langle J_\phi \rangle$ in Ignitor ($\langle J_\phi \rangle \simeq 9.3$ MA/m^2) should offer a considerable margin to attain the desired peak plasma density.
2. a high mean poloidal magnetic field ($\bar{B}_p \simeq 3.75$ T) and a correspondingly large toroidal plasma current ($I_p \simeq 12$ MA). High poloidal field can be sustained due to a combination of a strong toroidal magnetic field and an optimized plasma shape.
3. a low poloidal beta ($\beta_p = 8\pi\langle p \rangle/\bar{B}_p^2 \leq 0.15$ at ignition, where $\langle p \rangle$ is the volume-averaged plasma pressure).

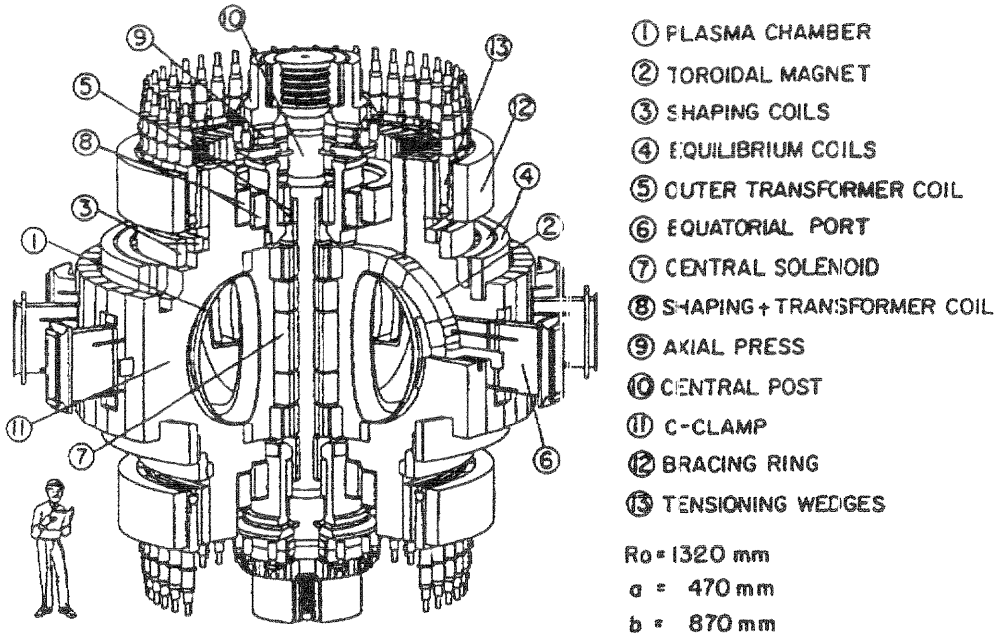

Fig. 1. Main components of the Ignitor UII machine.

4. a relatively small volume of the region where the magnetic safety factor q is less than unity.

The characteristics previously mentioned should lead to the following[4]:

1. a strong rate of ohmic heating up to ignition. This is accomplished by programming the initial rise of I_p and n_0 while gradually increasing the cross section of the plasma column. By the end of this relatively long ($t_{rise} \gtrsim 3$ to 4 s) transient phase, the electric field is strongly inhomogeneous (see Fig. 2). It is small at the center of the plasma column, where the temperature can achieve relatively high values and is maximum at the edge of the plasma column (corresponding to loop voltages $V_\phi \simeq 1$ V). This condition can be maintained even beyond ignition.

2. ignition at low temperature, corresponding to peak temperature $11 \lesssim T_0 \lesssim 15$ keV.

3. a limited degradation of the energy replacement time (τ_E) relative to that observed when injected heating is applied at discrete points around the torus, with a power much larger than the ohmic heating. The Ignitor strategy is to sustain a strong rate of ohmic heating up to relatively high temperatures, where fusion alpha-particle heating becomes significant. A comparable degradation of τ_E due to the alpha-particle heating is by no means certain as this form of heating is internal to the plasma and distributed axisymmetrically, two features it shares with ohmic heating

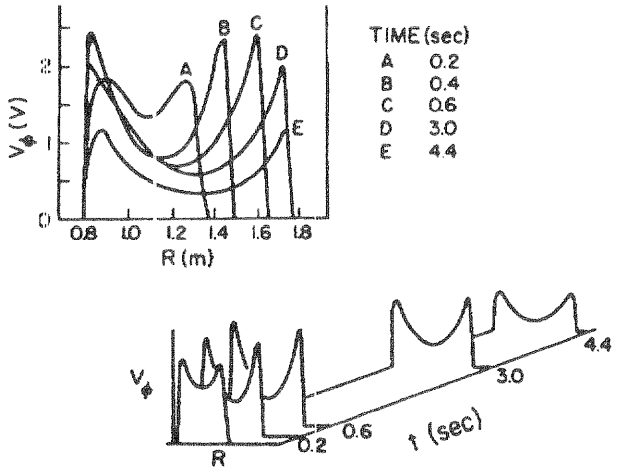

Fig. 2. Time evolution of the loop voltage, as a function of the plasma radius, for a typical 12-MA discharge.

that has optimal confinement characteristics. Thus, the degree of energy confinement required to attain ignition at low peak temperature ($T_0 \lesssim 15$ keV) with values of the confinement parameter $n_0\tau_E \gtrsim 4 \times 10^{20}$ s/m^3 should be reached with reasonable confidence.

4. a relatively high degree of purity that prevents dilution of the reacting nuclei and loss of internal energy from the plasma core by radiation. In practice, the plasma effective charge Z_{eff}

should not be higher than ~1.6 in the plasmas without auxiliary heating. A wide range of experiments performed so far have confirmed that Z_{eff} is a monotonically decreasing function of the plasma density. The high values of B_T and the low thermal loads on the first wall expected in Ignitor under low temperature ignition conditions are also favorable to obtain low values of Z_{eff}.

5. relatively high plasma edge densities that help to confine impurities to the scrape-off layer, where the induced radiation contributes to distribute the thermal wall loading more uniformly on the first wall.

6. good confinement of the plasma and of the alpha particles produced by the fusion reactions in the central part of the plasma column (a current $I_p \simeq 3$ to 4 MA is sufficient to confine the orbit of the 3.5-MeV alpha particles). The considerably larger currents Ignitor can produce confine the alpha particles and their associated heating to the central region, where the diffusion coefficient for the plasma thermal energy is consistently found to be minimal.

7. a paramagnetic plasma current I_θ (up to 9 MA), flowing in the poloidal direction that can increase the toroidal magnetic field B_T at $R = R_0$ up to ~11%.

8. a bootstrap current $I_{BS} \gtrsim 10\%$ of I_p at ignited conditions. This current slightly reduces the required magnetic flux variation to be produced by the poloidal magnet system.

9. a good margin for stability, in view of its low aspect ratio and of the low value of β_p at which Ignitor can operate, against ideal and resistive magnetohydrodynamic (MHD) modes and, in particular, against the onset of macroscopic internal $m^0 = 1$ (Ref. 13) modes that could hamper the attainment of ignition.[3]

Peaked plasma density profiles can be maintained by external means such as a pellet injector, if necessary. In fact, peaked profiles maintain stability against the so-called η_i modes that enhance the ion thermal transport.

I.C. Expected Plasma Parameters and Numerical Simulations

Recent results of free boundary numerical simulations[3-6] using the Tokamak Simulation Code (TSC) (Ref. 26) have shown that ignition is most effectively achieved soon after the end of the current rise. Favorable conditions are obtained in this phase of the discharge due to a broad toroidal current density profile (see Fig. 3). Then the region where $q < 1$ remains limited to a small fraction($< \frac{1}{10}$) of the total plasma volume.

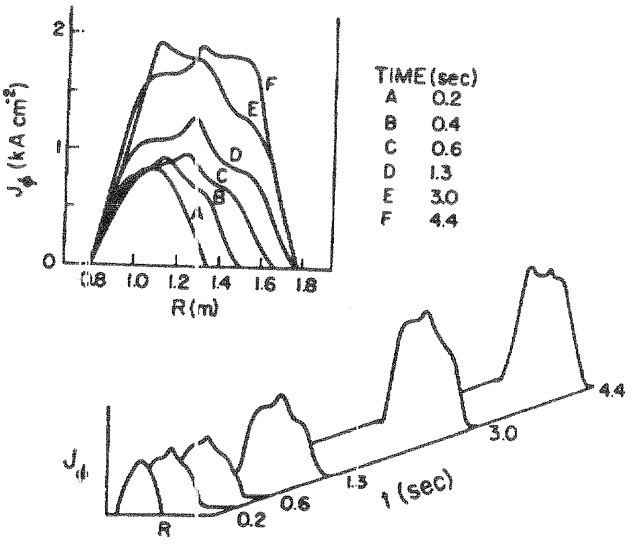

Fig. 3. Time evolution of the toroidal current density profile for the reference case of Table II, as a function of the plasma radius.

This strategy, combined with the low value of β_p that should prevent the onset of $m^0 = 1$ modes, minimizes the effects of potential sawtooth oscillations.

For the Ignitor parameters given in Table I (reference discharge), ignition can be reached[4] after a 3-s current ramp, at $t_{ignition} \simeq 4.3$ s, $T_0 \simeq 11$ keV, $\tau_E \simeq 0.66$ s, $n_{e0} \simeq 1.1 \times 10^{21}$ m^{-3}, and $n_{e0}/\langle n_e \rangle \simeq 2.2$, $\langle n_e \rangle$, being the volume average density, corresponding to a thermal stored energy $W \simeq 12$ MJ (details of the numerical results and the transport models used are given in Ref. 4). In this case, the peaking factor of the temperature profile $T_0/\langle T \rangle$ is about 3 (see Fig. 4), and $Z_{eff} \simeq 1.2$ is assumed to be constant over the plasma volume. The time evolution of the energy confinement time for the reference discharge is compared in Fig. 5 to estimates made from various global scalings.

We also notice that the alpha-particle heating power P_α (by definition equal to the total power losses P_L at ignition) is about 18 MW, while $P_{OH} \simeq 9.5$ MW (see Fig. 6). Thus, the thermal loading on the first wall is relatively mild.

During the current ramp, P_{OH} increases continuously while n_e is also being increased (see Figs. 6 and 7). The maximum ohmic heating power density is generated in a region off the magnetic axis (typically, around $r \simeq a/2$), where the temperature is relatively low. After the current ramp ends, P_{OH} falls gradually as the temperature rises, although not as quickly as the central voltage $V_{\phi 0} \sim T_0^{-3/2}$. The relatively large values of P_{OH} are due to the fact that, under nonstationary conditions, V_ϕ is a strong function of the plasma radius and is considerably higher at the edge than in the center. A set of results concerning this reference discharge is shown in Table II at three different times.

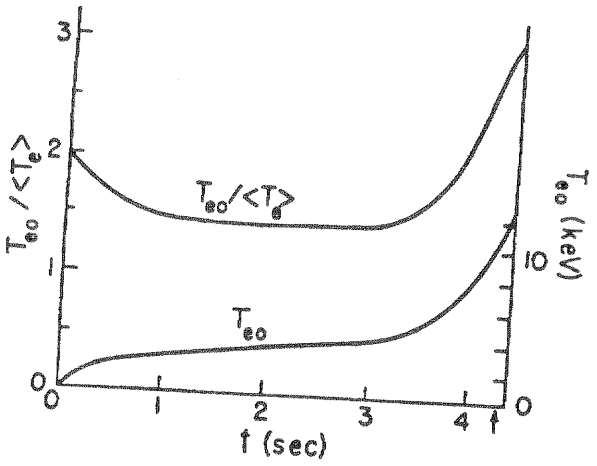

Fig. 4. Time evolution of the central ($T_{io} = T_{eo}$) and the ratio between peak- and volume-averaged temperature for the reference case of Table II. Ignition occurs at 4.3 s, marked by an arrow.

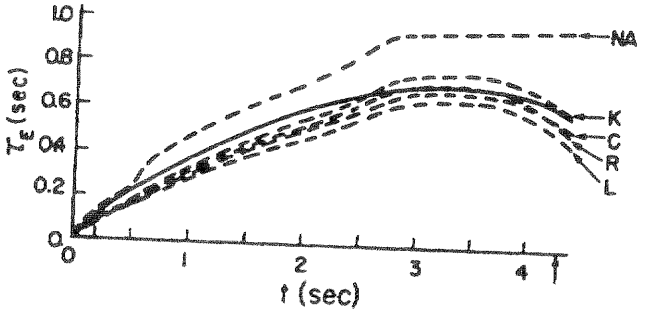

Fig. 5. Time evolution of the energy confinement time (solid line) for the reference case of Table II, compared to estimates made from various global scalings (broken curves). The scalings are NA, neo-Alcator[27]; K, Kaye All-Complex[28]; C, Coppi[29]; R, Rebut-Lallia[30]; and L, Lackner-Gottardi.[31]

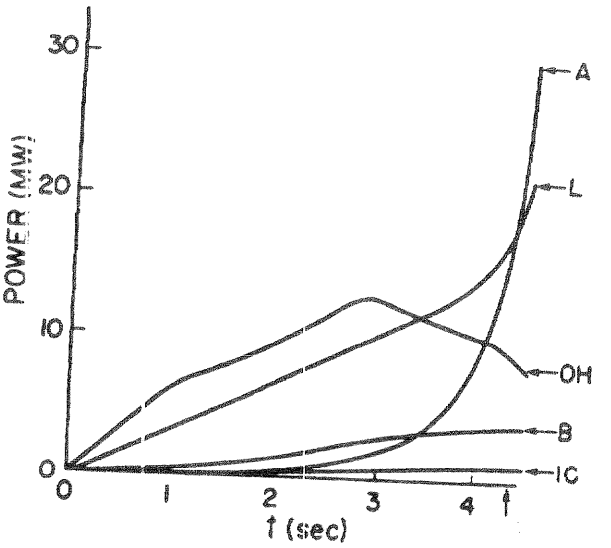

Fig. 6. Time evolution of the (volume integrated) heating and loss powers for the reference case of Table II. The powers are labeled as OH, ohmic heating; A, alpha-particle heating; L, total losses; B, bremsstrahlung radiation; IC, cyclotron and carbon impurity radiation ($Z_{eff} = 1.2$).

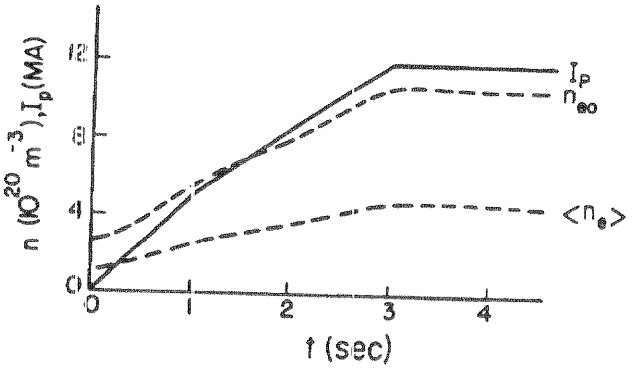

Fig. 7. Time evolution of the plasma current and the electron central and volume-averaged density for the reference case of Table II.

We notice that low temperature ignition is thermally unstable, since the plasma temperature tends to runaway (in principle), given the temperature dependence of the fusion reactivity. At the same time, it is not difficult to envision intrinsic plasma processes that may limit the temperature excursion. Among the external means we intend to employ are the injection of pellets, the compositions and sizes of which can be chosen so that the plasma temperature is not depressed to the point where fusion burning is quenched irreparably.

The maximum magnetic field $B_T \simeq 13$ T has been taken to have a flat top of 4 s while the maximum current $I_p \simeq 12$ MA has been assumed, for the reference design, to have a 3- to 4-s ramp and a flat top duration $\simeq 1$ s, followed by a gradual reduction of the current to 8 MA over 3 s. Our analyses indicate that greater values of I_p and the associated ohmic heating are not necessary in the ignited state as the fusion alpha-particle power takes care of the power balance. Moreover, as has been shown experimentally in TFTR (Ref. 32) and found by transport simulations of the Ignitor discharge,[4,10] the current density and the poloidal component of the field are not reduced in the central plasma region ($r \leq \frac{2}{3}a$) during the rampdown of the plasma current. Thus the confinement properties of the discharge are not expected to deteriorate relative to the case where the current is not decreased, as the TFTR experiments have indicated. By operating at lower I_p

TABLE II

Reference Discharge for the Ignitor Ult Machine*

	ST	*FT*	*IG*	
t (s)	0.2	3.0	4.3	Time
R_0 (m)	1.0	1.32	1.32	Major radius
a (m)	0.26	0.47	0.47	Minor radius
κ	1.07	1.87	1.87	Elongation
δ_G	0.08	0.42	0.43	Triangularity
$l_i/2$	0.47	0.32	0.4	Internal inductance
β_p	---	0.08	0.13	Poloidal beta
β (%)	0.06	0.8	1.26	Toroidal beta
n_{e0} (10^{20} m^{-3})	2.5	11.0	11.0	Peak electron density
$n_{\alpha 0}$ (10^{17} m^{-3})	---	1.5	12.0	Peak alpha-particle density
q_0	1.75	0.83	0.71	Central magnetic safety factor
q_ψ	4.2	3.3	3.6	Edge magnetic safety factor
$Vol_{q=1}$ (% of the total volume)	---	1.4	5.8	Volume inside the $q = 1$ surface
I_p (MA)	0.95	12.0	11.8	Toroidal plasma current
W (MJ)	0.07	7.5	11.7	Internal energy
T_0 (keV)	1.1	4.0	11.0	Peak electron temperature
τ_E (s)	0.13	0.71	0.66	Energy replacement time
P_{OH} (MW)	1.5	13.0	9.5	Ohmic power
P_α (MW)	---	2.0	17.8	Alpha-particle power
P_B (MW)	0.02	3.2	4.1	Bremsstrahlung radiation power
P_{IC} (MW)	0.01	0.4	0.5	Cyclotron and impurity radiation power
I_{BS} (MA)	---	0.6	1.0	Bootstrap current

*ST = start of the simulation; FT = beginning of the current flat top; IG = ignition.

and B_T, after ignition conditions are reached, it is possible to extend the time over which burning conditions can be sustained.

I.C.1. Energy Confinement at Ignition

In Table III, results are reported of simulations by the TSC for ohmic and ICRF heated discharges that show degraded confinement conditions relative to the reference discharge. In particular, in the first set of discharges, Z_{eff} has been increased from 1.2 (reference value) to 1.6. Note that both the auxiliary heated and the ohmic discharges reach ignition, if in the ohmic case,[4,10] the requirement of small $q < 1$ region is dropped on the theoretically based expectation that, for the relevant set of plasma parameters, the $m = 1$ modes that produce sawtooth oscillations are either stable or too weak to be significant. In the second set of discharges, the anomalous part of the ion thermal diffusion coefficient is increased by a factor of 3 relative to the reference discharge. With this assumption, the ohmic discharge does not reach ignition, and the parameters given in Table III (Ref. 5) are relative to the time when the maximum level of alpha-particle power production is reached. Instead, the discharge heated with ICRF power up to 15 MW reaches ignition at the end of the current ramp. This analysis shows that moderate amounts of auxiliary heating (Refs. 4 and 10), $P_{RF} \simeq 5$ to 15 MW, started during the current ramp, allow ignition with energy confinement time on the order of 0.4 s, while maintaining very small $q = 1$ regions well beyond ignition (Table III).

I.C.2. Plasma Density

For a given level of thermal transport and radiation losses (Z_{eff}), there is an optimum density that minimizes the time to reach ignition.[4,7,8,10] A higher density is necessary to compensate for degraded conditions. Higher densities, however, accelerate the toroidal current penetration by lowering the electron temperature and, consequently, produce a larger $q < 1$ region earlier (see Fig. 8). Furthermore, excessively large n_0 may lead to hollow temperature profiles during the current ramp, introducing a delay in the alpha-particle power production.

TABLE III

Ohmic and ICRF Heated Discharges That Show Degraded Confinement Conditions Relative to the Reference Discharge of Table II

	$Z_{eff} = 1.6$		Large Thermal Transport	
Heating	Ohmic	Injected	Ohmic[a]	Injected
P_{rf} (MW)	0	5[b]	0	15[c]
Z_{eff}	1.6	1.6	1.2	1.2
γ_i[d]	0.5	0.5	1.5	1.5
$t_{ignition}$ (s)	5.3	3.3	(5.0)	3.0
β_p	0.14	0.15	0.14	0.19
W (MJ)	12.8	14.0	12.9	16.6
T_0 (keV)	13.0	13.2	13.4	15.1
τ_E (ms)	570	555	470	425
P_{OH} (MW)	8.7	8.8	8.1	6.9
P_α (MW)	22.5	25.2	24.3	39.2
P_B (MW)	4.9	5.4	4.2	4.9
P_{IC} (MW)	1.0	1.1	0.5	0.7
$V_{q=1}$ (%)	>10	2.3	>10	1.4

[a]Subignited; never reaches ignition.
[b]$P_{rf} = 5$ MW for $t > 1.2$ s.
[c]$P_{rf} = 5$ MW for $1.2 < t < 1.8$ s; 10 MW for $1.8 < t < 2.4$ s; and 15 MW for $t > 2.4$ s.
[d]Ion thermal diffusion coefficient $\chi_i = \chi_i^{neo} + \gamma_i \chi_e^{nOH}$, where $\chi_e = \chi_e^{OH} + \chi_e^{nOH}$, reference $\gamma_i = 0.5$.

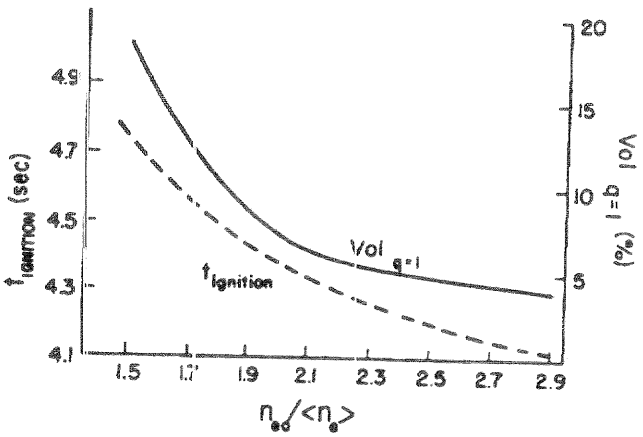

Fig. 8. Ignition time $t_{ignition}$ (broken curve) and volume $Vol_{q=1}$, inside the surface where $q = 1$, at ignition are shown, for cases that have the same initial conditions and current ramp as the reference case of Table II, as functions of the density profile for fixed electron peak density.

TABLE IV

Effects of Different Density Profiles

Density Profile	Narrow	Reference	Broad	Broad[a]
$n_{e0}/\langle n_e \rangle$	2.9	2.2	1.5	1.5
n_{e0} (10^{20} m^{-3})	11	11	11	8.4
$\langle n_e \rangle$ (10^{20} m^{-3})	3.8	5	7.3	5.6
$t_{ignition}$ (s)	4.1	4.3	4.7	4.3
W (MJ)	10.7	11.7	13.4	12.6
T_{e0} (keV)	11.2	11.0	11.1	13.0
β_p	0.12	0.13	0.15	0.15
τ_E (ms)	615	660	705	675
P_{OH} (MW)	8.8	9.5	9.9	9.1
P_α (MW)	17.4	17.8	19.0	18.7
P_B (MW)	3.2	4.1	5.8	4.2
P_{IC} (MW)	0.4	0.5	0.8	0.6
$V_{q=1}$ (%)	4.0	5.8	>10	4.8

[a]A lower density; $n_{e0} = 6.5 \times 10^{20}$ m^{-3}, at end of ramp ($t = 3$ s), increasing afterward is considered.

Broadening the density profile,[4,10] below $n_{e0}/\langle n_e \rangle = 2.2$ while keeping the same value of n_0 allows (ohmic) ignition at slightly higher values of τ_E and with a larger region where $q \leq 1$ (see Table IV and Fig. 9). Narrowing the density profile further produces only small improvements in ignition time and the size of the region where $q \leq 1$, but it allows ignition at smaller values of τ_E (see Table IV). Broad profiles at lower peak density n_0 give better ignition characteristics (last case, Table IV).

The effects of increasing n_0 during the current ramp or during the flat top have been investigated for different assumed levels of confinement degradation.[4,10] Better results are obtained by limiting n_0 to its reference value ($n_0 = 1 \times 10^{21}$ m^{-3}) at the end of the current ramp and, if needed, increasing its value during the flat top.

I.C.3. Injected Heating

A modest amount (e.g., 5 MW, see Table III) of injected heating, started during the initial current ramp (see Fig. 10), can shorten substantially the time to ignition by increasing the central heating. In addition, it effectively controls the size of the $q \leq 1$ region, by raising the temperature in the outer half of the plasma column and slowing down the rate of current penetration.[4,6,10] High temperatures in the central region, $T_0 = 10$ to 15 keV, act to "freeze in" the central current density. In all the cases where injected heating is present, the $q \leq 1$ region can be kept very small until well beyond ignition. In fact, this region is the result of the "tip" in the current density profile that is a

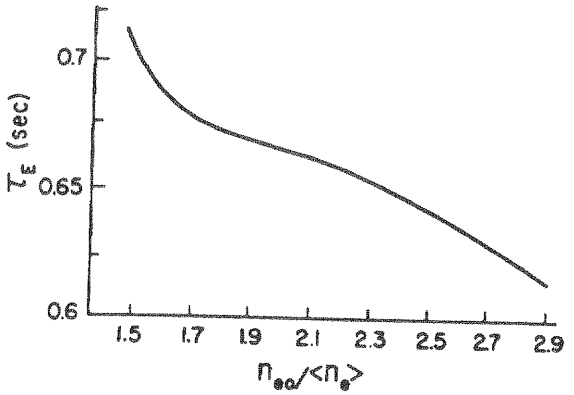

Fig. 9. Necessary energy confinement time, for ignition, as a function of the density profile at constant electron peak density. The initial conditions and the current ramp are assumed to be the same as those for the reference case illustrated in Table II.

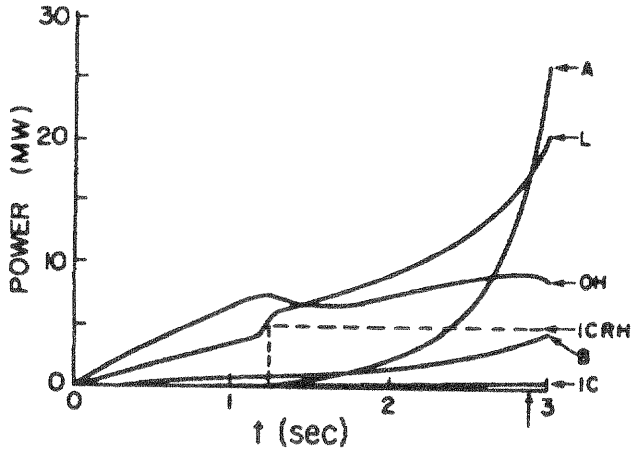

Fig. 10. Time evolution of the volume integrated powers for an Ignitor plasma with 5 MW of injected ICRF heating (shown by dashed line). Initial parameters and current ramp are the same as for the reference case of Table II. The powers are labeled as follows: OH, ohmic heating; A, alpha-particle heating; L, total losses; B, bremsstrahlung radiation; IC, cyclotron and carbon impurity radiation ($Z_{eff} = 1.2$).

consequence of the strict adoption of the neoclassical expression for the electrical resistivity. We do not consider the effect of the tip to be realistic.

I.C.4. Scenarios of Operation and Plasma Parameters

In Table V, we present the results for seven different scenarios of operation, with maximum plasma currents of 8, 10, and 12 MA, using different levels of injected heating power and different locations of the magnetic null point at the breakdown (i.e., initial plasma position close to the inner or outer edge of the limiter). The main parameters characterizing these scenarios and the corresponding plasma quantities (at ignition, or for subignited conditions when the maximum plasma temperature is reached) are given for $t_{ignition}$ (Ref. 33). The transport models used in these simulations, as well as all the other input parameters, are the same as for the reference discharge described[4] and reported for convenience as case 7 in Table V.

I.D. Experiments on the Second Stability Region

The access to the high-β second stability region[34] can be studied with plasmas that are far from fusion burn conditions. As is well known, these studies are important to identify the parameters of advanced fusion reactors. In order to analyze the relevant plasma regimes, Ignitor will be operated with relatively high values of q_ψ. The low aspect ratio ($\simeq$2.8) that characterizes this machine and its elongated plasma cross section make it particularly suitable to reach relevant finite-β conditions with interesting plasma parameters. In this case, ICRF has to be relied on as the primary heating system. In particular, in order to explore long pulse operation, the machine magnet currents can be lowered considerably relative to their reference design values. Since these magnets are cooled down to ~30 K and their ohmic heating can become minimal, Ignitor can be as useful as a superconducting facility in this respect. In fact, an impurity pumping system, to be used for extended duration (10 to 40 s) discharges, is being incorporated in the machine design.

I.E. D-^{3}He Fusion Burning Using ICRF Minority Heating in Ignitor

Ignitor has been designed to satisfy conditions where the 14.7-MeV protons and the 3.6-MeV alpha particles produced by the D-^{3}He reactions can supply thermal energy to a well-confined plasma. In particular, Ignitor can

1. sustain a plasma current exceeding that required ($I_p \gtrsim 6$ MA) to confine the proton orbits at birth
2. have more than sufficiently high densities so that the slowing-down time of both the protons and the alpha particles is shorter than the electron energy replacement time of the thermal plasma in which they are produced.

In order to boost the D-^{3}He fusion reaction rate, ion-cyclotron heating of a deuterium plasma with a ^{3}He minority can be used to create a tail in velocity space for the ^{3}He distribution function[35] with an optimal mean energy value. We note that the D-^{3}He fusion cross section has a maximum near $E \simeq 650$ keV for a helium beam incident on a deuterium target.

TABLE V

Different Operating Scenarios

	Case							
	1	2	3	4	5[a]	6	7	
I_p (MA)	8	8	10	10	10	12	12	Plasma current
	Out	Out	Out	Out	Out	Out	In	Location of the null
P_{rf} (MW)	0	10	0	10	0	0	0	Injected heating power
B_T (T)	10	10	11	11	11	13	13	Toroidal field at R_0
B_p (T)	4.4	4.4	5.5	5.5	5.5	6.5	6.5	Maximum poloidal field for $R < R_0$
B_p (T)	3.2	3.2	3.9	3.9	3.9	4.2	4.2	Maximum poloidal field for $R > R_0$
B_{vert} (T)	1.2	1.2	1.5	1.5	1.5	1.8	1.8	Vertical field at R_0
t_r (s)	3.0	3.0	3.5	3.5	3.5	4.0	3.0	Rampup time for I_p
$t_{ignition}$ (s)	6.0	4.0	5.6	5.0	5.5[b]	5.0[b]	4.3[b]	Ignition time
n_{e0} (10^{20} m^{-3})	8.0	8.0	9.0	9.0	9.0[b]	10.5[b]	10.5[b]	Peak electron density
T_0 (keV)	6.4	11.4	9.7	17.2	13.2[b]	11.8[b]	11.0[b]	Peak temperature
τ_E (s)	0.71	0.35	0.53	0.28	0.57[b]	0.59[b]	0.66[b]	Energy replacement time
P_α (MW)	2.3	10.3	10.8	38.0	20.0[b]	21.0[b]	17.8[b]	Alpha-particle power
P_{OH} (MW)	6.1	4.0	7.1	4.0	5.8[b]	8.9[b]	9.5[b]	Ohmic power
Z_{eff}	1.2	1.2	1.2	1.2	1.2	1.2	1.2	Effective charge
Q[c]	2.0	4.0	8.0	14.0	∞[b]	∞[b]	∞[b]	Performance parameter

[a]All the parameters are the same as those of case 3 except for the non-ohmic component of the anomalous thermal diffusion coefficient, which has been reduced by one-third. This is intended to represent a regime with mildly degraded confinement relative to the case where only "ohmic" transport is present.
[b]At ignition.
[c]$Q \equiv 5P_\alpha/(P_{OH} + P_{rf} - dW/dt)$ under transient conditions.

A preliminary analysis of the fusion power P_F that may be produced in Ignitor by this method indicates that $P_F \simeq 1$ MW may be reached, thanks primarily to the high value of the radio-frequency (rf) power density that can be coupled to the helium nuclei. We recall that in previous experiments, fusion power levels of 1.5 and 140 kW have been obtained in the Princeton Large Torus[36] and in the Joint European Torus[37] (JET), respectively. However, neither of these experiments had the currents and the particle densities required for the confinement and the slowing down of the 14.7-MeV protons.

Numerical simulations for this scenario in Ignitor were performed using the FPPRF code[38] that combines a ray tracing package with the solution of the Fokker-Planck equation for the minority species. Typical rf parameters were $P_{rf} = 18$ MW, $\nu = 132$ MHz, $\langle k_\parallel \rangle = 5$ to 10 m^{-1}. The parallel wavelength $\langle k_\parallel \rangle$ is estimated on the basis of the size of the adopted ICRF antennas. The ray tracing routine (SPRUCE) solves the dispersion relation for electromagnetic waves propagating in a hot plasma, while another set of routines evolves the distribution function of the minority ions in time by solving the bounce-averaged Fokker-Planck equation:

$$\frac{\partial f}{\partial t} = \langle Q \rangle + \langle C \rangle + \langle S \rangle \ ,$$

where $\langle Q \rangle$ represents the power deposition by the wave and is a quasilinear operator that computes the (spatially varying) resonant wave-particle energy exchange, $\langle C \rangle$ is the standard collision operator (involving pitch angle scattering, slowing down by electrons and background ions, and energy exchange with other species—electrons and ions), and $\langle S \rangle$ represents the combination of relevant sources and sinks (charge exchange, prompt losses of fast ions, . . .).

The code returns wave dispersion properties [in particular $N_\perp^2(r)$, where $N = kc/\omega$ is the index of refraction], the rf power deposition profile as a function of r and θ, the minority ion distribution function $f(r, E, \mu)$, the mean energy of the rf heated minority as a function of r, as well as an estimate of the beam-target fusion reaction yield (i.e., number of protons per second for the case of D-^{3}He where the "beam" is composed of ^{3}He ions and the "target" of deuterium ions). The code is able to treat the interaction with the minority species at either the fundamental or the first harmonic of the cyclotron frequency.

In the minority heating scenario for the fast wave, four characteristic distances can be identified that are important for the damping of the wave. In terms of $x = R - R_{mag}$ (where $R_{mag} \simeq R_0$ is the distance of the magnetic axis from the symmetry axis), these are

1. $x_c = 0$, the distance of the cyclotron resonance $\omega = \Omega_{He}$ of the helium ions (note that the wave field at this location has mostly a right-handed polarization, which is opposite to the one required for optimal coupling with the ion gyromotion).

2. $\Delta x_c = (k_\parallel V_{th,He}/\omega)R_{mag}$, the width of the thermal broadening of the cyclotron resonance.

3. $x_L \simeq -(\frac{1}{2})(n_{^3He}/n_e)R_{mag}$, the distance of $N_\parallel^2 = L \simeq \Sigma_i(\omega_{pi}/\Omega_{ci})^2\Omega_{ci}/(\Omega_{ci} - \omega)$ cut-off surface $k_\perp^2 = 0$ [the other cut-off surface, $N_\parallel^2 = R \simeq \Sigma_i(\omega_{pi}/\Omega_{ci})^2\Omega_{ci}/(\Omega_{ci} + \omega)$, is located near the plasma periphery]. In the cold plasma approximation, at x_L the wave has a complete left-hand polarization.

4. $x_S \simeq -(\frac{7}{12})(n_{^3He}/n_e)R_{mag}$, the distance of $N_\parallel^2 = S \equiv (R + L)/2$ ion hybrid resonance surface $k_\perp^2 \to \infty$. When the effects of finite plasma temperature are taken into account, the (electromagnetic) fast wave can couple to the (electrostatic, short wavelength) ion Berstein wave (mode conversion) near the ion hybrid surface leading to a heating of the bulk plasma.

When the ICRF is applied in the minority heating regime, it is important that

1. the evanescent region separating the cutoff and ion hybrid resonance surfaces be as large as possible in order to minimize direct heating of the bulk plasma via mode conversion (we find that the addition of a small concentration of a third ion species—hydrogen or tritium—is helpful in this respect)

2. the width $|\Delta x_c|$ be broad enough to overlap the cutoff surface where optimal conditions of wave field polarization for coupling with helium gyromotion are encountered.

As the helium is heated from the initial plasma temperature to effective tail temperature of 1 MeV (or more), the width $|\Delta x_c|$ is seen to increase from 0.01 to 0.1 m, finally overlapping the cutoff region. Accordingly, the peak in $\mathrm{Im}(N_\perp)$, associated with the damping of the wave, moves from its original position at the cyclotron resonance toward the $N_\parallel^2 = L$ cutoff surface.

The helium distribution function is obtained, at several times during the simulation, and the relevant level lines in the $(v_\parallel, v_\perp)$ plane, show the characteristic[38] two-horn shape with values of the relevant pitch angle ~60 to 80 deg. Analytically, f can be described by a combination of a core Maxwellian and an anisotropic tail with a characteristic perpendicular mean energy[35] given by

$$T_{eff} = T_e[1 + (\tfrac{3}{2})\xi_{rf}] \ .$$

Here the $\xi_{rf} = \langle \rho_{rf} \rangle \tau_s/(3n_{He}T_e)$, where τ_s is the slowing-down time of the helium nuclei, and ρ_{rf} is the local value of rf power density coupled to them. Therefore

$$\xi_{rf} = \frac{\hat{T}_e^{1/2}}{\hat{n}_e \hat{n}_{He} \ln \hat{\Lambda}} \left(\frac{\langle \rho_{rf} \rangle}{\mathrm{MW/m^3}} \right) ,$$

when written in practical units ($\hat{T} = T/10$ keV, $\hat{n} = n/10^{20}$ m^{-3}, $\ln \hat{\Lambda} = \ln \Lambda/10$).

Figures 11 and 12 show the rf power deposited into the plasma and the helium mean energy as functions of the minor radius for the case of maximum fusion reactivity referring to a plasma with $n_{e0} = 2.5 \times 10^{20}$ m^{-3}, $T_{e0} = 20$ keV, $T_{i0} = 15$ keV, $n_{^3He0}/n_{e0} = 7\%$, and $n_{T0}/n_{e0} = 5\%$. Generally, over 95% of the rf power is deposited (promptly) into the helium. A substantial fraction of this power (up to 50%) is then transferred to the electrons by collisional processes.

The fusion power output is estimated with several simplifying assumptions (e.g., an isotropic velocity distribution function for the fast ions), and the quoted value $P_F \simeq 1$ MW should be considered as tentative at this time. Work is continuing in order to identify the relevant optimal conditions.

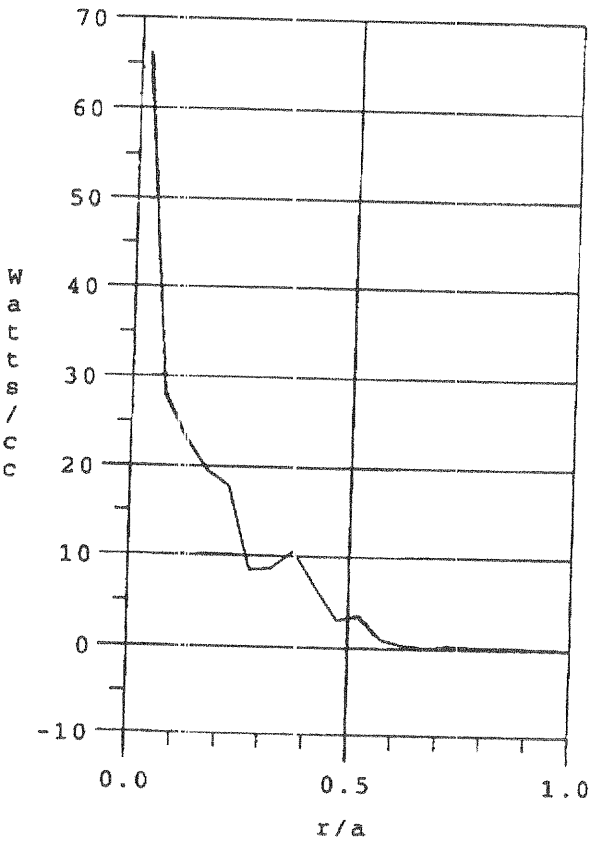

Fig. 11. The rf power deposition profile for minority D-^{3}He acceleration. The rf power input is 18 MW.

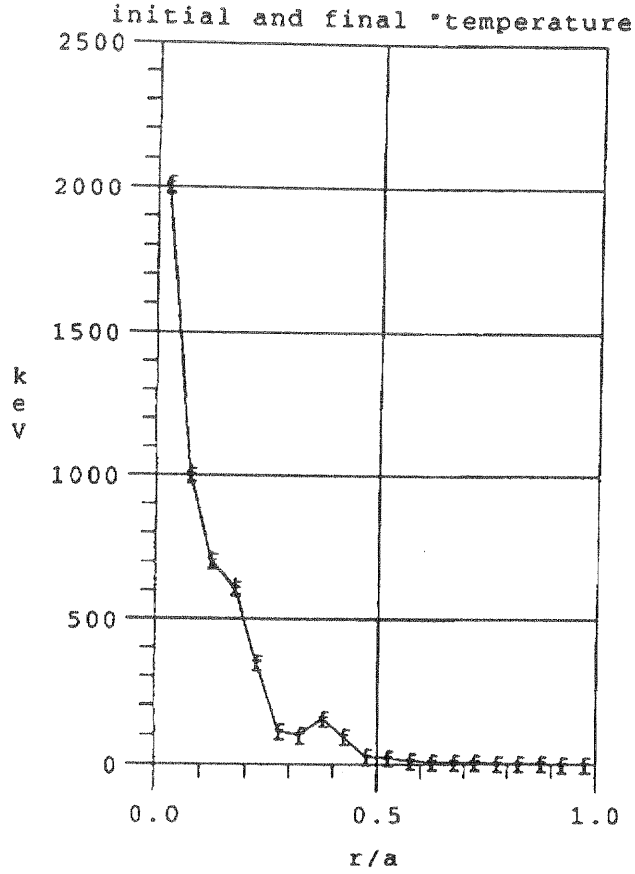

Fig. 12. Mean energy acquired by the minority (^{3}He) nuclei with an rf power input of 18 MW. The labels "initial" and "final" refer to stages in the numerical iteration.

Alternatively, we have also computed the D-^{3}He reactivity parameter $\langle \sigma v \rangle_F$ for a ^{3}He distribution function as given by Stix.[35] The relevant two-dimensional velocity space integral is computed numerically. In Fig. 13, we show $\langle \sigma v \rangle_F$ as a function of ξ_{rf} for different values of the bulk plasma temperatures, T_e and T_i. We note that for a given set of temperatures, there is an optimal value of ξ_{rf} for which $\langle \sigma v \rangle_F$ is maximum, and this value can be lowered considerably by increasing T_e and T_i as shown in Fig. 13. Since ξ_{rf} is inversely proportional to the square of the electron density (for constant minority concentration), while $P_F \propto n_{He} n_D \langle \sigma v \rangle_F$, an increase in the bulk plasma temperature allows a higher optimal density at constant values of ρ_{rf} and therefore of P_F.

A zero-dimensional (no quantitative radial profile effect included) estimate of the total fusion power can be obtained from $\langle \sigma v \rangle_F$ in the following way. On the basis of the inferred value of $\langle \rho_{rf} \rangle$, we can select, for given temperatures, an optimal density product $\hat{n}_e \hat{n}_{He}$. This is determined in such a way that the corresponding value of ξ_{rf} is the one for which $\langle \sigma v \rangle_F$ is maximum, i.e., $\langle \sigma v \rangle_F^{max} \simeq 2.0 \times 10^{-22}$ m^2/s. Then assuming that these optimal conditions can be produced only in a small fraction V_{eff} of the total plasma volume [say $V_{eff} \simeq (1/25)V$], we estimate

$$P_F \simeq 6(\hat{n}_D \hat{n}_{He})^{optimal} \times (V_{eff}/\text{m}^3)\ \text{MW} .$$

In the case where $T_e = 20$ keV, $T_i = 15$ keV for example, and $\langle \rho_{rf} \rangle = 65$ MW/m^3 over V_{eff}, we find $\hat{n}_e^{optimal} \simeq 2.5$ and $\hat{n}_{He}^{optimal} \simeq 0.2$, so that $P_F \simeq 1$ MW. This value is in reasonable agreement with that obtained from the code FPPRF under similar conditions.

II. THE CANDOR EXPERIMENT

The criteria that have been followed for the design and construction of the key components of the Ignitor machine have also been used to identify the parameters and carry out feasibility studies of a high field experiment that was proposed at first in 1980 with the intent to reach D-^{3}He fusion burn conditions[39] on the basis of existing technologies and knowledge of plasma physics. This is called Candor[39] and is capable of producing plasma currents up to 25 MA with toroidal magnetic fields $B_T \simeq 13$ T. Unlike Ignitor, Candor would operate with values of β_p around unity and the central part of the plasma column in the Second Stability Region. The D-^{3}He ignition regime can be reached by a combination of ICRF heating and alpha-particle heating due to D-T fusion reactions that take the role of a trigger.

The reference plasma dimensions and parameters of Candor are reported in Table VI and the reference plasma parameters in Table VII.

The machine's key elements are shown in Fig. 14. Note that the toroidal field coils are divided into two

TABLE VI

Reference Design Parameters of the Candor Machine

$R_0 \simeq 2.1$ m	Major radius of the plasma column
$a \times b \simeq 0.92 \times 1.75$ m^2	Minor radii of the plasma cross section
$\delta_G \simeq 0.36$	Triangularity of the plasma cross section
$I_p \lesssim 25$ MA	Plasma current in the toroidal direction
$B_T \simeq 13$ T	Vacuum toroidal field at R_0
$\langle J_\phi \rangle \lesssim 4.7$ MA/m^2	Average toroidal current density
$\bar{B}_p \lesssim 3.8$ T	Mean poloidal field
$I_p \bar{B}_p \lesssim 96$ MN/m	Confinement strength parameter
$q_\psi \simeq 3.9$	Edge magnetic safety factor at $I_p = 25$ MA
$\Phi_T \simeq 160$ V·s	Total poloidal flux requirement
$V_0 \simeq 80$ m^3	Plasma volume
$S_0 \simeq 150$ m^2	Plasma surface area

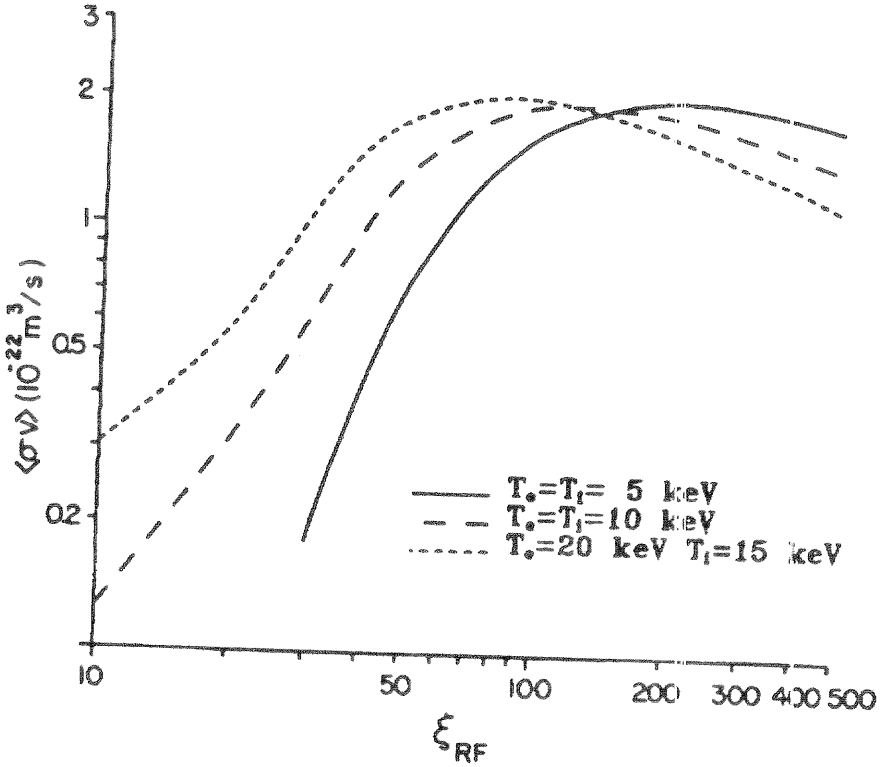

Fig. 13. Reactivity parameter $\langle\sigma v\rangle_F$ as a function of the ξ_{rf} that characterizes the ^{3}He distribution function; different values for the bulk plasma temperatures T_e, T_i are considered.

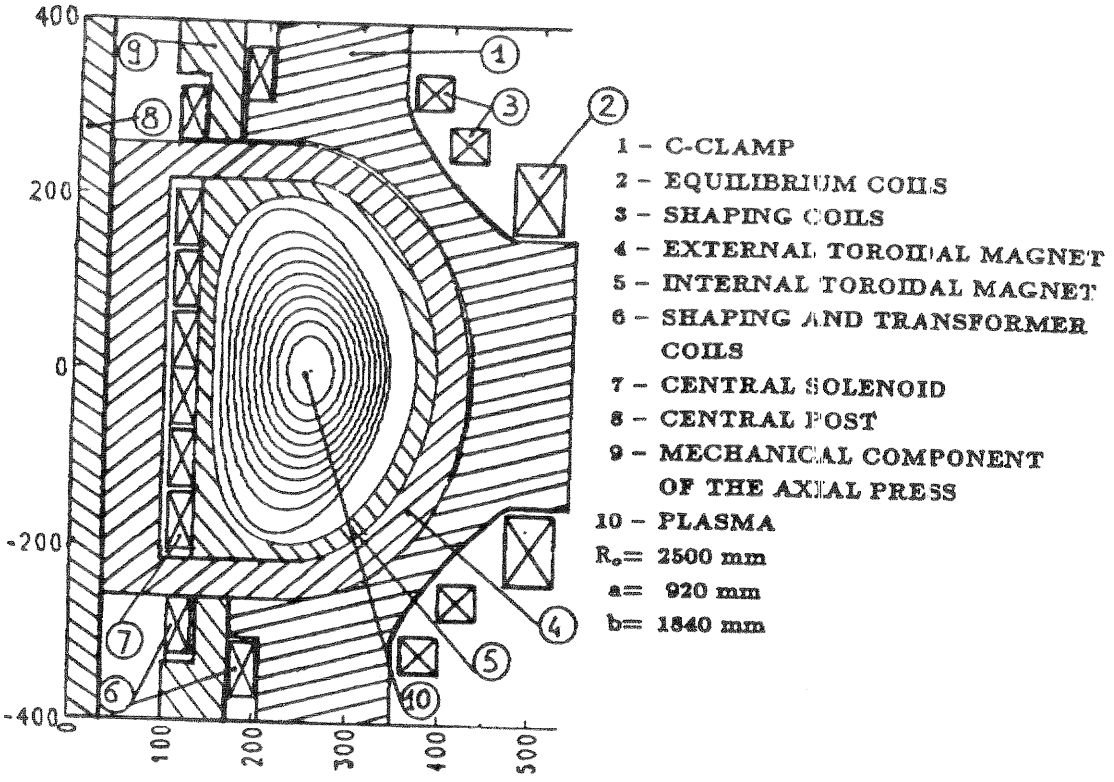

Fig. 14. Main components of the Candor machine.

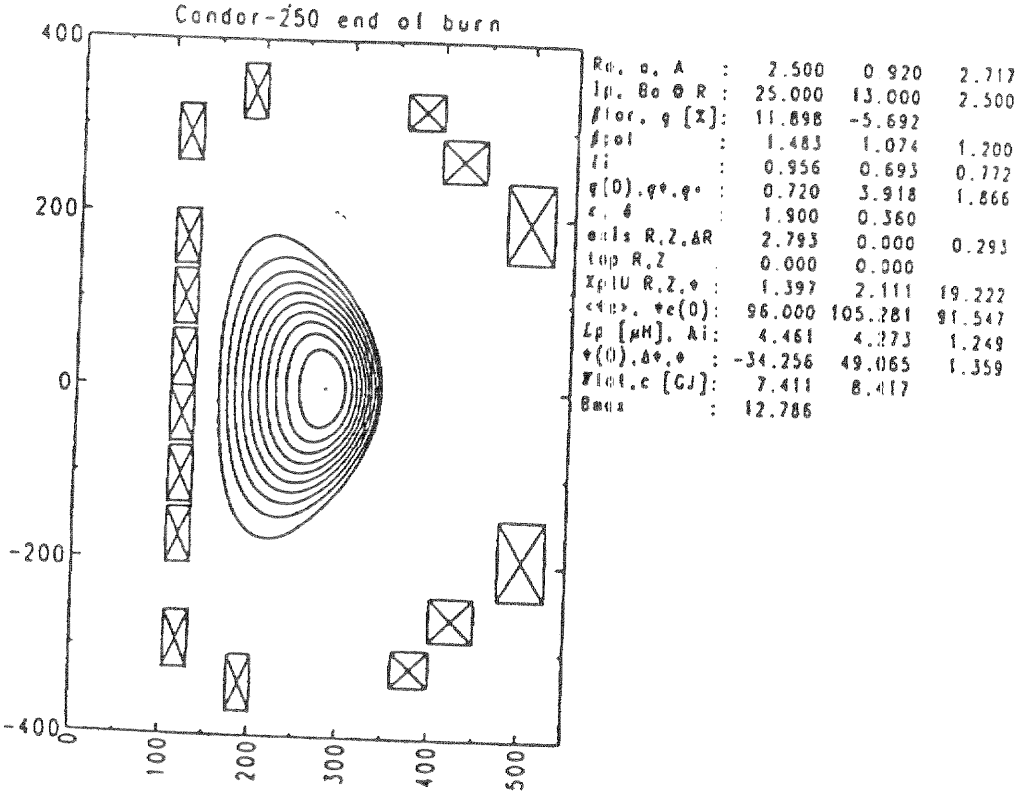

Fig. 15. MHD equilibrium configuration for the end of burn in Candor. The value of $\beta_{tor} = 11.9\%$ corresponds to a peak plasma pressure $p_0 = 400$ atm.

TABLE VII

Reference Plasma Parameters for the Candor Experiment

$T_0 = 65$ keV	Peak plasma temperature
$n_{e0} = 2 \times 10^{21}$ m^{-3}	Peak electron density
$p_0 = 400$ atm	Peak plasma pressure
$\beta_p = 1.2$	Poloidal beta
$W = 1$ GJ	Internal energy

sets of coils and that the central solenoid (air core transformer) is placed between the two sets of toroidal field coils. Ignitor instead has the classical configuration involving only one set of toroidal field coils that surround the central solenoid. As indicated in Table VI, the poloidal magnetic flux variation Φ_T necessary to induce a current of 25 MA in Candor is large. The linked magnetic configuration adopted for the Candor design combined with the larger dimensions, when compared to Ignitor, makes it possible to produce the desired values of Φ_T with lower current densities (by more than a factor of 2) in both the toroidal and poloidal field coils. Therefore assuming that the magnets operate in

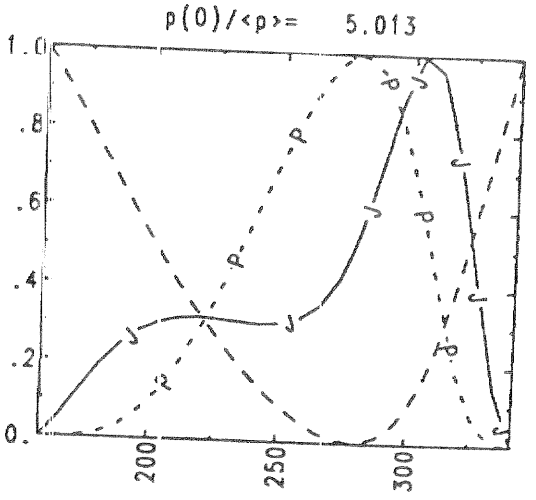

Fig. 16. Pressure, current density, and poloidal flux profiles in atomic units as a function of the major radius for the plasma configuration of Fig. 15.

the same temperature range as those of Ignitor, the characteristic times over which the plasma discharge can be sustained are longer by more than a factor of 4. Among the drawbacks of the linked-magnet solutions,

we may single out the need of reliable joints for the external set of toroidal field coils.

In Fig. 15, we show the MHD equilibrium configuration, obtained by using the TEQ code,[40] with 25 MA of plasma current. This situation arises at the end of the burn; the corresponding pressure, current density, and poloidal flux profiles are indicated in Fig. 16.

ACKNOWLEDGMENTS

This work was supported in part by the U.S. Department of Energy and by ENEA of Italy. Many thanks are due G. Hammett for making his code available to us and for his advice and to R. Budny for verifying some of our numerical results.

REFERENCES

1. B. COPPI, "High Current Density Tritium Burner," RLE PRR-75/18, Massachusetts Institute of Technology (1975); see also *Comments Plasma Phys. Controlled Fusion*, 3, 2 (1977).

2. B. COPPI and F. PEGORARO, "Salient Characteristics of the Ignitor Experiment," *Il Nuovo Cimento*, 9D, 691 (1987).

3. B. COPPI et al., "Current Density Transport, Confinement and Fusion Burn Conditions," *Proc. 13th Int. Conf. Plasma Physics and Controlled Nuclear Fusion Research*, Washington D.C., October 1–6, 1990, Vol. 2, p. 337, International Atomic Energy Agency (1991).

4. B. COPPI, M. NASSI, and L. E. SUGIYAMA, "Physics Basis for Compact Ignition Experiments," *Phys. Scripta*, 45, 112 (1992).

5. B. COPPI, L. E. SUGIYAMA, and M. NASSI, "Plasma Characteristics for a Compact D-T Ignition Experiment," *Fusion Technol.*, 21, 1612 (1992).

6. L. E. SUGIYAMA and M. NASSI, "Free Boundary Current Ramp and Current Profile Control in a D-T Ignition Experiment," *Nucl. Fusion*, 32, 387 (1992).

7. A. AIROLDI and G. CENACCHI, "Sensitivity Studies on Ignition in Ignitor," *Fusion Technol.*, 19, 78 (1991).

8. A. AIROLDI and G. CENACCHI, "Ignition Prospects for Ignitor," *Plasma Phys. Controlled Fusion*, 33, 91 (1991).

9. B. COPPI et al., "Quiescent Window for Global Plasma Modes," *Phys. Rev. Lett.*, 63, 2733 (1989).

10. B. COPPI et al., "Reconnection and Transport in High Temperature Regimes," *Proc. 14th Int. Conf. Plasma Physics and Controlled Nuclear Fusion Research*, Wurzburg, Germany, September 30–October 7, 1992, Paper-CN-56/3-1, Vol. 2. p. 131, International Atomic Energy Agency, Vienna (1993).

11. W. A. HOULBERG, Oak Ridge National Laboratory, Private Communication (1992).

12. A. AIROLDI and G. CENACCHI, "Effects of Sawtooth Activity in Ignitor," *Plasma Phys. Controlled Fusion*, 34, 1493 (1992).

13. A. C. COPPI and B. COPPI, "Stability of Global Modes in Advanced Plasma Confinement Configurations," *Nucl. Fusion*, 32, 205 (1992).

14. R. BETTI and J. R. FREIDBERG, "Stability of Alfvén Gap Modes in Burning Plasmas," *Phys. Fluids B*, 4, 1465 (1992).

15. M. NASSI et al., "Range of Objectives of the Ignitor Experiments," presented at Int. Sherwood Theory Mtg., Newport, Rhode Island, March 29–31, 1993.

16. F. CARPIGNANO et al., "ICRF System and Plasma Performance of the Ignitor Experiments," presented at 10th Topl. Conf. Radio-Frequency Power in Plasma, Boston, Massachusetts, 1993.

17. B. COPPI and L. LANZAVECCHIA, "Compact Ignition Experiments Physics and Design Issues," *Comments Plasma Phys. Controlled Fusion*, 11, 47 (1987).

18. B. COPPI, "Direct Approach to Achieving Ignition Conditions," *Vuoto*, 18, 153 (1988).

19. B. COPPI and the IGNITOR GROUP, "Characteristics and Expected Performance of the Ignitor-U Experiment," *Proc. 12th Int. Conf. Plasma Physics and Controlled Nuclear Fusion Research*, Nice, France, October 10–11, 1988, Vol. 3, p. 357, International Atomic Energy Agency (1989).

20. "Ignitor Project Feasibility Study," The Ignitor Program Group, status report November 27, 1988, ENEA (1989).

21. A. ANGELINI, B. COPPI, and M. NASSI, "Compact Ignition Experiments: Design and Performance," *Proc. 14th Symp. Fusion Engineering*, San Diego, California, September 30–October 3, 1991, Vol. 1, p. 411, Institute of Electrical and Electronics Engineers (1992).

22. G. CENACCHI, B. COPPI, and L. LANZAVECCHIA, "Magnetohydrodynamic Equilibria and Poloidal Field System for Ignitor-Ult," RTI/INN (92) 16, ENEA (1992).

23. B. COPPI, M. NASSI, and L. E. SUGIYAMA, "Engineering Characteristics of the Ignitor Ult Experiment," *Fusion Technol.*, 21, 1607 (1992).

24. B. COPPI, M. NASSI, and the IGNITOR PROJECT GROUP, "Physics Criteria and Design Solutions for an Advanced Ignition Experiment," *Proc. 17th Symp. Fusion Technology*, Rome, Italy, September 14–18, 1992, Vol. 2, p. 162, C. FERRO, M. GASPAROTTO, H. KNOEPFEL, Eds., North Holland Publishing Company (1993).

25. G. J. BOXMAN et al., "Low and High Density Operation of Alcator," *Proc. 7th European Conf. Plasma Physics,*

September 1-5, 1975, Vol. 2, p. 14, Ecole Polytechnique Fédérale de Lausanne, Switzerland (1976).

26. S. C. JARDIN, N. POMPHREY, and J. DELUCIA, "Dynamic Modelling of Transport and Positional Control in Tokamaks," *J. Comput. Phys.*, **66**, 481 (1986).

27. R. J. GOLDSTON, "Energy Confinement Scaling in Tokamaks: Some Implications of Recent Experiments with Ohmic and Strong Auxiliary Heating," *Plasma Phys. Controlled Fusion*, **26**, 87 (1984).

28. S. M. KAYE et al., "Status of Global Energy Confinement Studies," *Phys. Fluids*, **2**, 2926 (1990).

29. B. COPPI, "Transport Coefficients for the Plasma Thermal Energy and Empirical Scaling 'Laws,'" *Comments Plasma Phys. Controlled Fusion*, **12**, 319 (1989).

30. P. H. REBUT, P. P. LALLIA, and M. L. WATKINS, "The Critical Temperature Gradient Model of Plasma Transport: Applications to JET and Future Tokamaks," *Proc. 12th Int. Conf. Plasma Physics and Controlled Nuclear Fusion Research*, Nice, France, October 10-11, 1988, Vol. 2, p. 191, International Atomic Energy Agency (1989).

31. K. LACKNER and N. A. O. GOTTARDI, "Tokamak Confinement in Relation to Plateau Scaling," *Nucl. Fusion*, **30**, 767 (1990).

32. M. E. MAUEL et al., "Achieving High Fusion Reactivity in High Poloidal Beta Discharges in TFTR," *Proc. 14th Int. Conf. Plasma Physics and Controlled Nuclear Fusion Research*, Wurzburg, Germany, September 30-October 7, 1992, Papers CN-56/A-3-4, Vol. 1, p. 205, International Atomic Energy Agency (1993).

33. M. NASSI, "Poloidal Flux Requirement: Analysis and Application to the Ignitor Configuration," *Fusion Technol.*, **24**, 50 (1993).

34. B. COPPI et al., "Ideal-MHD Stability of Finite-Beta Plasma," *Nucl. Fusion*, **19**, 715 (1979); see also PRR(R.L.E.) 78/24, Massachusetts Institute of Technology (1978).

35. T. H. STIX, "Fast Wave Heating of a Two Components Plasma," *Nucl. Fusion*, **15**, 737 (1975).

36. R. E. CHRIEN and J. D. STRACHAN, "D-^{3}He Reaction Measurements During Fast Wave Minority Heating in the PLT Tokamak Experiment," *Phys. Fluids*, **26**, 1953 (1983).

37. J. JAQUINOT, G. J. SADLER, and the JET TEAM, "D-^{3}He Fusion in the Joint European Torus Tokamak—Recent Experimental Results," *Fusion Technol.*, **21**, 2254 (1992).

38. G. W. HAMMETT, "Fast Ion Studies of Ion Cyclotron Heating in the PLT Tokamak," PhD Thesis, Princeton University (1986).

39. B. COPPI, "Physics of Neutronless Fusion Reacting Plasmas," *Phys. Scripta*, **T212**, 590 (1982).

40. L. D. PEARLSTEIN, Lawrence Livermore National Laboratory, Private Communication (1992).